



Impact of Tropical Cyclone Avoidance on Fishing Vessel Activity over Coastal China Based on Automatic Identification System Data during 2013–2018

Weihua Fang^{1,2,3,4} · Cunmin Guo^{1,2,4} · Yinan Han^{1,2,4} · Rongfa Qing^{1,2,4}

Accepted: 22 June 2022 / Published online: 8 August 2022
© The Author(s) 2022

Abstract Tropical cyclones (TCs) may cause severe impacts on the activities of coastal fishing vessels. Due to the unavailability or unacceptability of detailed Automatic Identification System (AIS) data that are capable of differentiating fishing activity from navigation, as well as the lack of detailed models and observation data of TC winds, few studies have provided quantitative and reliable assessment of the impacts of TCs on fishing activities. In this study, we modeled snapshots for the TC winds of 52 TCs over the Northwest Pacific (NWP) basin from 2013 to 2018, as well as daily fishing hours and daily hours of presence (hereafter “vessel hours”) of fishing vessels. Based on these data, the spatiotemporal pattern of fishing vessel activity over offshore China was first analyzed and mapped. Then, a TC wind hazard index and absolute and relative impact indices were proposed to assess the impact of the 52 TCs on fishing and vessel hours. Their relationship was then fitted with the cumulative distribution function (CDF) of the log-normal distribution. The results show that in the 2013–2018 period, the most active fishing areas were located in the South China Sea. In each instance, an increase was first observed in the initial several years; then a decrease followed in the yearly

total fishing hours per vessel in the remaining years. The relative impact index was significantly correlated to the TC wind hazard index proposed in this study. Based on the quantitative relationship between the specified TC hazard index and the impact indices, it is possible to implement a pre-cyclone rapid loss assessment due to TC avoidance in the future.

Keywords Fishing hours · Fishing moratorium · Impact index · Tropical cyclone · Vessel hours

1 Introduction

Tropical cyclone (TC) disasters may have severe impacts on the activities of coastal fishing vessels. China’s total marine economic output value reached CNY 8.34 trillion (about USD 1.26 trillion) in 2018, and the contribution rate of fisheries exceeded 50% (MNR 2019). At the same time, marine fisheries in China face the threat of TC disasters in the Northwest Pacific (NWP) every year. In 2017, disasters in China caused direct economic losses to fisheries of approximately CNY 17.36 billion (about USD 2.57 billion), of which 64.3% were caused by TCs (MARA 2018a). Approximately 80–100 TCs are generated every year around the world, and approximately 1/3 are generated in the NWP (Fang and Shi 2012). About eight TCs make landfall on the China mainland every year in average. It is necessary to clarify the spatial and temporal patterns of China’s marine fishing vessel activities and to quantify the impact of TCs on them.

Detailed Automatic Identification System (AIS) data, capable of distinguishing between fishing activity and sailing to and from fishing grounds, are difficult to access. Most existing studies of the spatiotemporal patterns of fishing

✉ Weihua Fang
weihua.fang@bnu.edu.cn

¹ Key Laboratory of Environmental Change and Natural Disasters, Ministry of Education, Beijing Normal University, Beijing 100875, China
² Faculty of Geographical Science, Beijing Normal University, Beijing 100875, China
³ Southern Marine Science and Engineering Guangdong Laboratory, Guangzhou 511458, China
⁴ Academy of Disaster Reduction and Emergency Management, Ministry of Emergency Management and Ministry of Education, Beijing 100875, China

vessel activities have been based on data from public reports or datasets such as the yearbooks of the Food and Agricultural Organization of the United Nations (FAO). These data sources include global annual fishing vessel information on the country scale (Anticamara et al. 2011). However, spatially explicit maps of fishing efforts over different months or seasons remain unavailable (Guet et al. 2019). Some researchers have tried to use the gravity model, which distributes total fishing effort to units, like grounds or cells, based on a weighted index of attractiveness or importance that varies among different units, to reconstruct the global spatial distribution of fishing activities (Gelchu and Pauly 2007; Watson et al. 2013). This method can only estimate theoretical fishing activities, based on the assumption that fishing activities are determined by the defined weighted index. Thus, it is still difficult to quantify a realistic, detailed picture of fishing activities (Yu et al. 2014).

Consequently, studies on losses to the fishing industry caused by TCs have mostly focused on direct losses, such as shipwrecks and damage to onshore processing and storage facilities, while little attention has been paid to the losses due to fishing suspension and production reduction. For example, some studies have evaluated direct losses based on field survey data, such as the number of shipwrecks in specific research areas, while there are few quantitative assessments of the losses caused by the suspension of fishing vessel activities (Xu et al. 2005; Monteclaro et al. 2018). Although some studies have taken into account indicators of fishermen's income loss due to the suspension of fishing vessel activities, most of these efforts have been based on statistical data available in provincial or national units (Ren 2009; Han et al. 2016). Few have used dynamic tracking data of fishing vessels to identify the patterns of fishing vessel activities during a specific TC, but when undertaken these efforts have lacked quantitative assessments (Zheng et al. 2016). The common problem of such studies is the lack of both quantitative and dynamic analyses on fishing activity reduction during TC events. It is difficult to meet the requirements of dynamic and quantitative indirect loss assessment.

In recent years, the application of vessel monitoring systems (VMSs) and AIS has made it possible to quantify real-time fishing vessel activities at high spatial resolutions. Researchers have integrated global AIS data, and have quantitatively estimated the distribution of global daily fishing vessel activity intensity. The spatial resolution of the results has reached approximately 1 km (Kroodsma et al. 2018). This dataset provides support for further clarification of the spatial and temporal characteristics of regional fishing vessel activities and enables a dynamic assessment of the impact of TCs on fishing vessel activities.

Based on this dataset, our study had two goals. The first was to quantitatively analyze the spatiotemporal characteristics of fishing vessel activities throughout China's coastal

area. The other was to quantitatively analyze the impact of TCs on China's offshore fishing vessel activities. Specifically, we first obtained the global daily fishing vessel activity distribution product based on AIS data and analyzed the spatiotemporal characteristics of fishing vessel activities in the offshore areas of China from 2013 to 2018. Then, we defined two absolute impact indices and two relative impact indices of a single TC on fishing vessel activities. This enabled us to quantitatively analyze the impact of 52 TCs on fishing and vessel activities near China's offshore during the 6 years between 2013 and 2018. Our study provides support for understanding the large-scale tendencies of fishing vessel activities as well as a basis to dynamically and quantitatively assess the indirect losses to fisheries caused by TCs.

2 Materials

The study area covers the main fishing areas near the coastline of China. The data used in this study mainly include the historical TC track and intensity dataset and daily fishing hours (total hours that all vessels were fishing in the specific grid cell during a day) and vessel hours (total hours that all vessels were present in the specific grid cell during a day) dataset. Based on the two variables, fishing ratio, which is the ratio of fishing hours to vessel hours, has been calculated to reflect the overall utilization efficiency of fishing vessels.

2.1 Fishing Moratorium in the Study Area

The study area is defined as the sea area within the extent of 105°E–128°E and 17°N–42°N. Due to China's seasonal fishing moratorium policy, fishing activities in the study area are suspended from approximately May to September every year. According to the regulations of the Ministry of Agriculture of China, the starting and ending times of the fishing moratorium are shown in Table 1. The boundaries of the different fishing moratorium zones are shown with white dotted lines in Fig. 1, where Line #1 and Line #2 are 35°N and 26.5°N, respectively. Line #3 is the Fujian-Guangdong

Table 1 Fishing moratorium in the study area

Year	Region	Starting time	Ending time
2013–2016	North of Line #1	06/01 12:00	09/01 12:00
	Line #1 to Line #2	06/01 12:00	09/16 12:00
	Line #2 to Line #3	05/16 12:00	08/01 12:00
	South of Line #3	05/16 12:00	08/01 12:00
2017–2018	North of Line #1	05/01 12:00	09/01 12:00
	Line #1 to Line #2	05/01 12:00	09/16 12:00
	Line #2 to Line #3	05/01 12:00	08/16 12:00
	South of Line #3	05/01 12:00	08/16 12:00

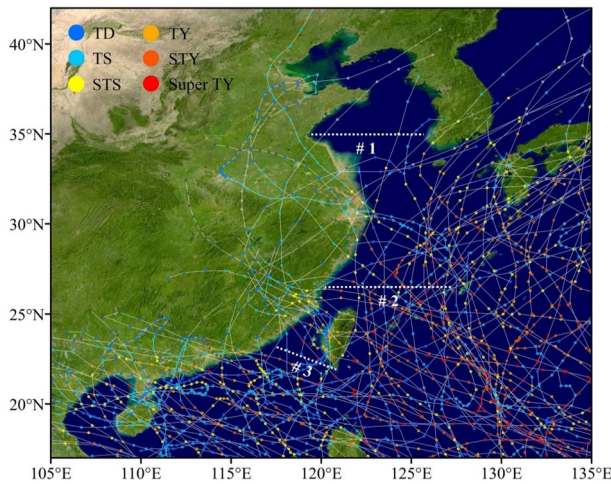


Fig. 1 Tropical cyclone (TC) best track dataset during 2013–2018 and boundaries regulated by the fishing moratorium policy of China. TD: tropical depression ($10.8 \leq$ maximum wind speed, MWS ≤ 17.1 m/s), TS: tropical storm ($17.2 \leq$ MWS ≤ 24.4 m/s), STS: super tropical storm ($24.5 \leq$ MWS ≤ 32.6 m/s), TY: typhoon ($32.7 \leq$ MWS ≤ 41.4 m/s), STY: severe typhoon ($41.5 \leq$ MWS ≤ 50.9 m/s), Super TY: super typhoon (MWS ≥ 51.0 m/s). Lines # 1–3 are the boundaries of different fishing moratorium zones according to MARA (2018b).

Sea Boundary Line, which is the connection line between ($117^{\circ}31'37.40''\text{E}$, $23^{\circ}09'42.60''\text{N}$) and ($120^{\circ}50'43''\text{E}$, $21^{\circ}54'15''\text{N}$) (MARA 2018b).

2.2 Best Tracks in the Northwest Pacific (NWP)

Two data sources were used. One is the best track dataset of historical TCs in the NWP from the China Meteorological Administration (CMA), as shown in Fig. 1 (Ying et al. 2014). The other source is the International Best Track Archive for Climate Stewardship (IBTrACS) from the World Meteorological Organization (WMO) (Knapp et al. 2010). The information used in the CMA dataset includes the central positions of TCs every six hours (part of observation intervals are three hours after 2017) and the central minimum pressure. The information used in the WMO data includes the wind radii of the TC track points observed by the Joint Typhoon Warning Center (JTWC).

2.3 Fishing Vessel Activities in the Northwest Pacific (NWP)

The dataset of global gridded daily fishing hours and vessel hours by Kroodsma et al. was used in this study. This dataset is derived from tens of billions of AIS records around the world since 2012, using convolutional neural network (CNN) methods to distinguish between the fishing and

non-fishing status of fishing vessels with an overall accuracy greater than 90% (Kroodsma et al. 2018).

The main information of the dataset includes gear types, flags, daily fishing hours (t_f) (Fig. 2c, d), daily vessel hours (t_v) (Fig. 2a, b), and the Maritime Mobile Service Identity (MMSI) of fishing vessels present in every grid. The spatial resolution of the data is 0.01° , and the temporal resolution is one day.

3 Methods

In order to analyze the fishing activity patterns and quantify the relationship between TC hazard and its impact on fishing hours and vessel hours, this study defined the fishing activity intensity indicator, the TC impact index (including absolute and relative indices) on fishing activities, TC hazard index, and the fitting function.

3.1 Spatiotemporal Patterns of Fishing Vessel Activities

To analyze the interannual and intra-annual changes in fishing vessel activities in the study area, the average total fishing hours and vessel hours per vessel (mt_f and mt_v , respectively) were calculated by year and by month using Eq. 1.

$$mt_{f/v} = \text{Sum}\{t_{f/v} \text{ of all grid cells in the study area}\} / N, \quad (1)$$

where N is the total number of fishing vessels present in the study area during the calculation year or month; t_f , t_v are daily fishing hours and vessel hours in each 0.01° grid cell, respectively.

3.2 Impact of Tropical Cyclones (TCs) on Fishing Vessel Activities

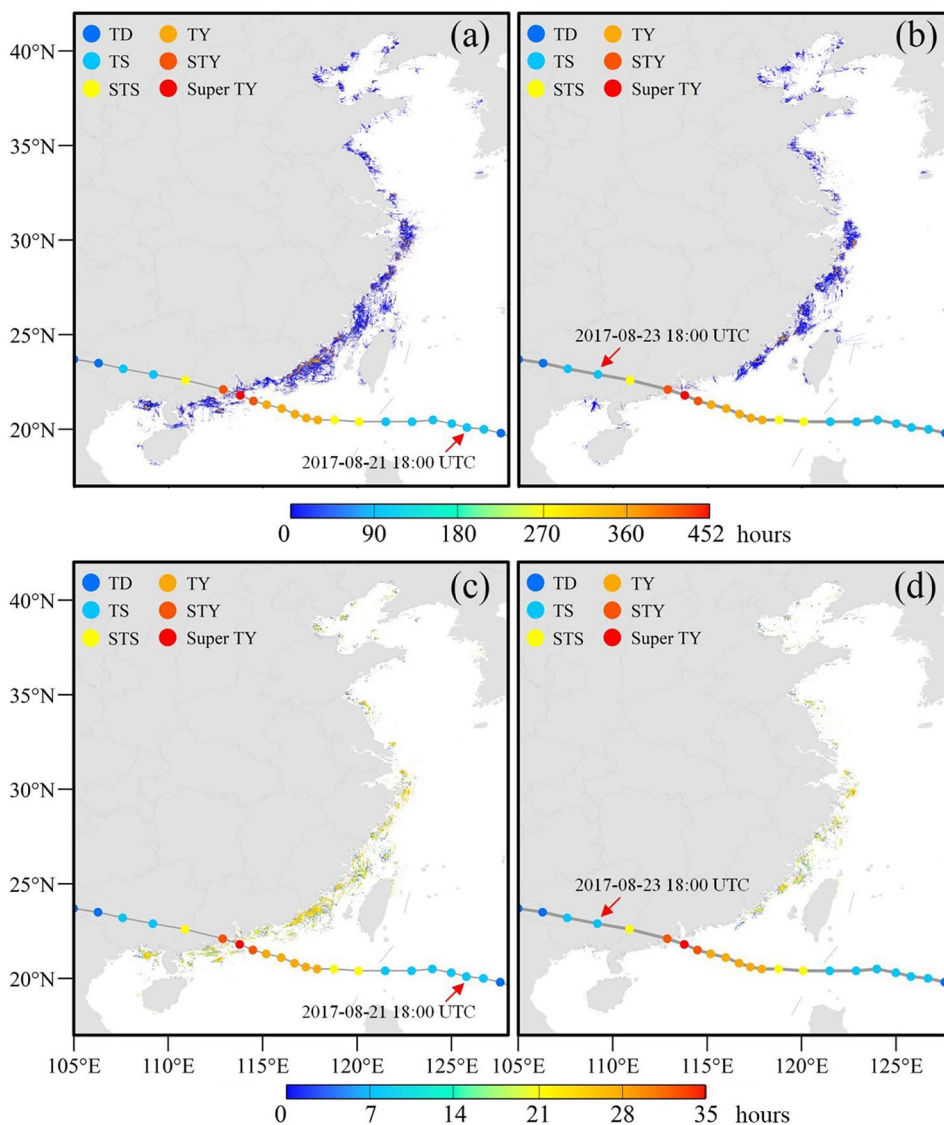
Before defining the TC absolute/relative impact indices, the impact area was first defined. Then the baseline fishing hours and vessel hours were calculated to reflect the reference value under nondisaster conditions.

3.2.1 Boundary of the Impacted Area

According to the standard from CMA on issuing weather warning signals, the Blue warning for TCs will be issued if vessels might or have been affected by a TC within 24 hours and the maximum gust wind speed has been greater than the minimum wind speed of Beaufort scale eight (17.2 m/s). Under this circumstance, fishing vessels are required to take a detour or return to harbor (CMA 2007).

In actual situations, the impacted area of TCs on fishing vessel activities should be greater than the scale eight wind radius range for two main reasons: (1) errors might exist

Fig. 2 Daily vessel hour distribution t_v and fishing hour distribution t_f in two days during tropical cyclone Hato in 2017: **a** t_v on 2017-08-21 UTC; **b** t_v on 2017-08-23 UTC; **c** t_f on 2017-08-21 UTC; **d** t_f on 2017-08-23 UTC. For each grid cell, t_f and t_v refer to total fishing and vessel hours of all vessels present in this grid cell during a single day, respectively.



in the prediction of TC tracks; and (2) fishermen outside the forecasted scale eight wind radius will also take proactive measures for the purpose of risk prevention. In previous studies, an empirical method to delineate the boundary of the area impacted by TCs was to use the 500 km buffer zone (Elsberry 1987; Ren et al. 2007). Considering the two problems mentioned above, the radius of the TC-impacted area was determined to be 500 km.

3.2.2 Impact Indices of Tropical Cyclones (TCs) on Fishing Vessel Activities

The first step is to specify TC's impact start and end dates. The TC's impact start date is the first day that the TC center reaches the 48 hour forecast area regulated by CMA. The boundary of the 48 hour forecast area is the line linked by (34°N, 132°E)–(22°N, 132°E)–(15°N, 125°E)–(15°N, 110°E)

(China Weather 2010). The TC's impact end date is the day that a TC goes beyond 500 km from the China land boundary after its landfall.

The second step is to define the baseline vessel hours b_v and fishing hours b_f during a TC. With reference to the definition used by the World Bank (Jovel and Mudahar 2010), b_f and b_v represent the assumed t_f and t_v under nondisaster conditions. In this study, the average t_f and t_v within 10 days before a TC's impact starts and 10 days after TC's impact ends are calculated as b_f and b_v , respectively. The formulas are as follows:

$$b_f = \sum_{i=1}^{10} (t_{f(d_0-i)} - t_{f(d_1+i)}) / 20, \tag{2}$$

$$b_v = \sum_{i=1}^{10} (t_{v(d_0-i)} - t_{v(d_1+i)})/20, \tag{3}$$

where $t_{f(d)}$ (Fig. 3b) and $t_{v(d)}$ represent the daily fishing hours and daily vessel hours on the date d ; d_0 represents the TC’s impact start date; and d_1 represents the TC’s impact end date.

The second step is to define the absolute impact indices Δt_v and Δt_f which refer to the total reduction in vessel hours and fishing hours, respectively, during a TC in each grid of the impacted area (Fig. 3c), as compared to the baseline hours. For each TC, Δt_v and Δt_f are calculated as follows:

$$\Delta t_f = \sum_{i=0}^{D-1} (t_{f(d_0+i)} - b_f), \tag{4}$$

$$\Delta t_v = \sum_{i=0}^{D-1} (t_{v(d_0+i)} - b_v), \tag{5}$$

where b_v and b_f (Fig. 3a) are the baseline vessel hours and baseline fishing hours during the TC, respectively; and D is the total number of TC impact days.

We then calculate the maximum reduction rate of the total fishing hours and total vessel hours, respectively, across the impacted area during the TC. For each TC, the variations in T_v and T_f with time (Fig. 4) are first constructed, where T_v and T_f are the sum of t_v and t_f values of all grids in the impacted area for each day, respectively; then, the baseline values B_f and B_v (Fig. 4) are calculated using a similar method as mentioned before; next, the minimum values of T_f and T_v during the TC are identified, and their relative reduction rate to B_f and B_v is calculated. The results are relative impact index on fishing hours (IR_f) and relative impact index on vessel hours (IR_v), as shown in Eqs. 8 and 9, respectively.

$$B_f = \sum_{i=1}^{10} (T_{f(d_0-i)} - T_{f(d_1+i)})/20, \tag{6}$$

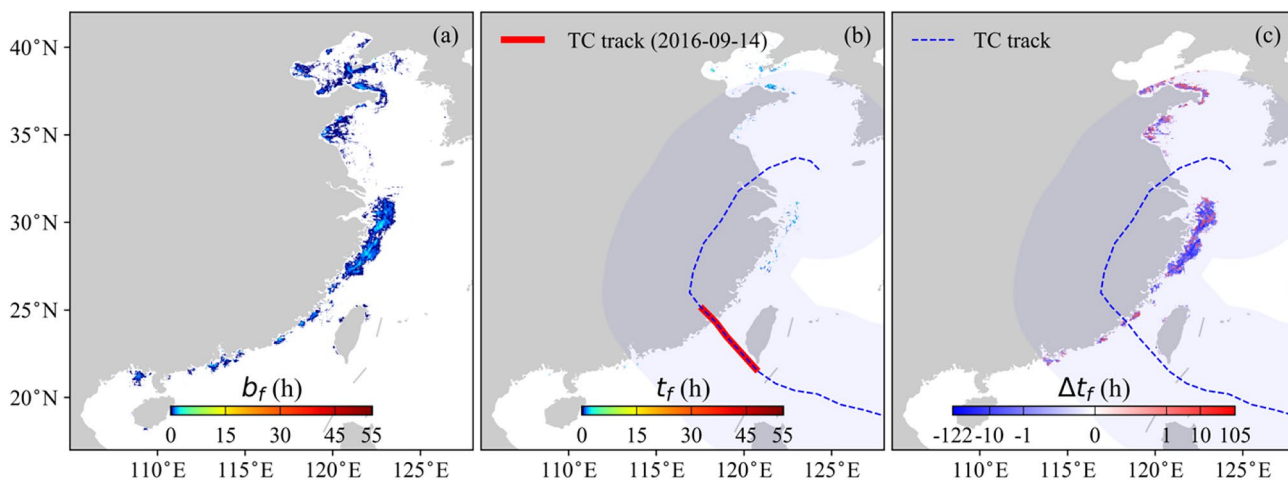
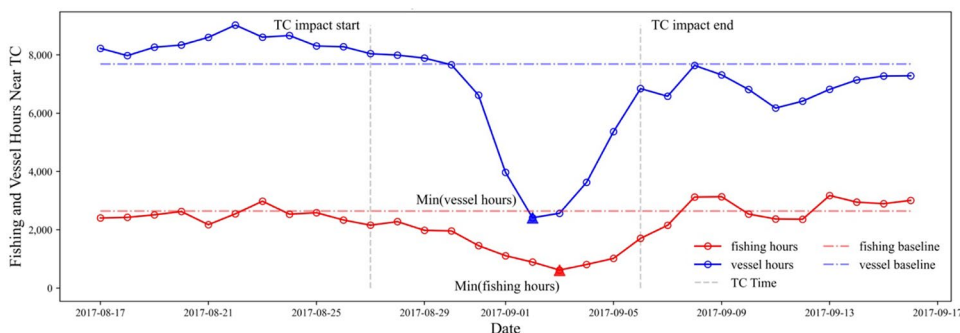


Fig. 3 Procedure for assessing September 2016 tropical cyclone Meranti’s impact on fishing hours. **a** Baseline fishing hours b_f before and after the occurrence of Meranti; **b** daily fishing hours t_f during

Meranti on 2016-9-14 for example; **c** absolute impact index Δt_f of Meranti on fishing hours.

Fig. 4 Variations in T_v and T_f with time during a tropical cyclone (TC)



$$B_v = \sum_{i=1}^{10} (T_{v(d_0-i)} - T_{v(d_1+i)})/20, \quad (7)$$

$$IR_f = 1 - \text{Min}\{T_{f(d_0+i)} | i = 0, 1, 2, \dots, D-1\} / B_f, \quad (8)$$

$$IR_v = 1 - \text{Min}\{T_{v(d_0+i)} | i = 0, 1, 2, \dots, D-1\} / B_v, \quad (9)$$

where $T_{f(d)}$ and $T_{v(d)}$ are T_f and T_v on the date d , respectively; d_0 and d_1 are the dates of TC impact start and impact end, respectively (grey dashed lines in Fig. 4); D is the total number of TC impact days.

When calculating the baseline, if part of the subject days is within the fishing moratorium period, the B_f and B_v are separately calculated for the moratorium status and non-moratorium status. For example, the B_f for the moratorium status is the average T_f in all moratorium days within 10 days before TC's impact start and 10 days after TC's impact end. Then the IR_f and IR_v should be separately calculated depending on whether the dates on which T_v and T_f reach the minimum are in moratorium status or not. That means if the minimum T_f is in fishing moratorium status, the IR_f should be the relative reduction rate to B_f to account for the moratorium status.

3.3 Quantification of the Tropical Cyclone (TC) Wind Hazard Intensity

Existing indices for measuring the TC wind hazard usually include the Accumulated Cyclone Energy (ACE), the Power Dissipation Index (PDI) (Emanuel 2005), the Chicago Mercantile Exchange Hurricane Index (CHI) (CME Group 2009), and the Willis Hurricane Index (WHI) (Owens and Holland 2010). Among these indices, the ACE and PDI consider the maximum wind speed (MWS) and duration of TCs. The CHI adds the maximum wind speed radius based on the ACE and PDI. The WHI further considers the moving speed of TC centers. Based on these indices, Li and Fang (2012) developed the Rapid Loss Index (RLI) to rapidly assess losses.

For all the indices mentioned above, the MWS is used to reflect the instantaneous maximum wind speed in a TC. However, the MWS is not able to reflect the spatial distribution of the instantaneous wind speed field, which should be considered to assess TC wind hazards more accurately. Parametric wind field models can improve the hazard indices by quickly simulating the instantaneous spatial distribution of the TC wind speed field in any specified resolution (Tan and Fang 2018).

Following the parametric wind field model combination for the NWP in Tan and Fang (2018), an advanced

accumulated spatiotemporal cyclone wind hazard index (CWI) is proposed. First, a 1 km instantaneous wind field is simulated for each point of a TC track with a time interval of 6 hours. The Georgiou gradient model (Georgiou et al. 1983) was used to simulate the asymmetry of the TC gradient wind field and the Yan Meng boundary model (Meng et al. 1997) was used to convert gradient winds to surface winds at a height of 10 m by considering the effects of surface roughness. The input parameters include TC locations (longitudes and latitudes), the minimum central pressure (Pc), TC heading speed (C), TC heading direction (Vd), the maximum wind radius (RMW), the Holland shape parameter (B), and surface roughness (Z0), which assumes that the surface roughness is uniform and equal to a sea surface roughness of 0.0003 m). All the parameters can be found in the CMA best track dataset except for the RMW and B. We used the statistic model by Lin and Fang (2013) to calculate RMW and the Vickery model (Vickery and Wadhwa 2008) to calculate B. Then, the simulated surface wind speed field for each point is spatially integrated to reflect the TC's instantaneous intensity. Finally, the CWI is obtained by integrating the instantaneous intensities of all 6 hour TC points. The CWI takes into account the duration, moving speed, spatial distribution of the wind speed, and area impacted by TCs. The formula is as follows:

$$CWI = \int_T \left(\frac{C}{C_0} \right) \int_A \left(\frac{V}{V_0} \right)^2 dAdT, \quad (10)$$

where T represents the duration from TC's impact start date to the impact end date (in 6 h intervals); A represents the distribution area of the instantaneous wind speed field for each TC point; V represents the simulated wind speed at each grid in the instantaneous wind field (wind speed greater than scale six or 10.8 m/s is selected); C represents the moving speed of TC centers; V_0 represents the reference value of the wind speed, which is set as 33.44 m/s (Owens and Holland 2010); and C_0 represents the reference value of the TC moving speed, which is set as 18 km/h (Lin and Fang 2013).

3.4 Relationship between Impact Indices and Hazard Index

First, the correlation coefficients between the TC relative impact indices (IR_f and IR_v) and the TC hazard index CWI were analyzed. The Pearson correlation coefficient and Spearman rank correlation coefficient were used.

Second, there are two main steps to quantify the relationship between the TC impact indices and the hazard index. One is to select a proper function for fitting curves. Another is to quantify the uncertainty by using the upper and lower bounds of the standard deviation intervals (Mo and Fang 2016).

There are two main principles for selecting the fitting function: one is that the value domain should be $[0, 1]$ and the function should be monotonically increasing. Another is an acceptable goodness of fit. According to the distribution characteristics of the data of the research results, the cumulative distribution function (CDF) of the log-normal distribution is selected as the fitting function (Porter 2021). The formula is as follows:

$$F(x; \mu, \sigma) = \phi\left(\frac{\ln x - \mu}{\sigma}\right) = \int_0^x \frac{1}{\sigma\sqrt{2\pi}} \cdot \frac{1}{z} \exp\left(-\frac{(\ln z - \mu)^2}{2\sigma^2}\right) dz, \quad (11)$$

where ϕ is the CDF of the standard normal distribution, and μ and σ are the parameters.

4 Results

Based on the materials and methods, the temporal and spatial changes or patterns are first analyzed. Then the absolute and relative impact indices of 52 historical TCs are calculated and analyzed. Meanwhile, the TC hazard index for each TC is also modeled, after which the relationship between the TC impact indices and the TC hazard index is fitted using the log-normal CDF. Key details of all the results above are presented in this section.

4.1 Spatiotemporal Patterns of Fishing Vessel Activities

In this section, the yearly and monthly total fishing hours and vessel hours per vessel across the study area have been analyzed first. Then the gridded hours summed by year and by month are plotted.

4.1.1 Temporal Patterns

The yearly total fishing hours and vessel hours per vessel in the study area (that is, yearly mt_f and mt_v , respectively) during 2013–2018 are shown in Fig. 5a. The annual mt_f values increased initially, and then decreased after 2015. One possible reason is that China has adjusted its policies on fuel subsidies for fisheries since 2015 for the sake of reducing marine fishing intensity and conserving fishery resources (MOF 2015). The fishing ratio (fishing hours versus total vessel use hours per vessel per day or month or season) fluctuates slightly around approximately 25%.

The monthly total fishing hours and vessel hours per vessel in the study area (that is, monthly mt_f and mt_v , respectively) during 2013–2018 are shown in Fig. 5b. Both indicators reach the maximum in September, and the minimum mt_f is in June, while the minimum mt_v is in February. The results suggest strong seasonality in both fishing hours and vessel hours. For fishing hours, the results follow the order

of autumn > spring > winter > summer. For vessel hours, the results follow the order of autumn > spring > summer > winter. The main reason for the low fishing hours in summer is China's fishing moratorium policies (Table 1). The fishing ratio shows an upward trend from January to May and reaches a maximum of approximately 40% in May. Then, it drops from May to July, with a minimum of approximately 23%. From August to December, it recovers to a relatively stable level of approximately 34%.

The yearly and monthly total fishing hours per vessel in the four seas of China are shown in Fig. 6. The highest yearly fishing hours per vessel are in the South China Sea. Compared to 2013, the total fishing hours per vessel in 2018 dropped by 19.4%, 4.0%, 7.5%, and 18.6% in the Bohai Sea, Yellow Sea, East China Sea, and South China Sea, respectively. The monthly total fishing hours per vessel across the four seas are substantially different in May, August, and December. In other months, monthly total fishing hours per vessel across the four seas are close.

4.1.2 Spatial Patterns

The spatial patterns of the yearly total fishing hours are shown in Fig. 7a. In the Bohai Sea, the fishing hotspot areas are scattered and have partially expanded since 2016, mainly near the southern coastline of Hebei Province. In the Yellow Sea, the fishing hotspot areas are mainly distributed near the Shandong Peninsula and have expanded significantly since 2016. In the East China Sea, the most widely distributed fishing hotspot area of the entire study area has suffered a sharp contraction since 2017. In the South China Sea, fishing hotspots are mainly distributed quite close to the coastline and have slightly expanded since 2016.

The spatial patterns of the yearly total vessel hours are shown in Fig. 7b, and the results resemble the patterns of fishing hours. During 2013–2015, the East China Sea area near the coastlines of Jiangsu Province, Zhejiang Province, and Shanghai was basically the most widely distributed hotspot area. After 2016, the vessel hour hotspot areas in the Bohai Sea, Yellow Sea, and South China Sea expanded slightly, while those in the East China Sea contracted significantly.

The spatial patterns of the monthly total fishing hours (aggregated by month during 2013–2018) are shown in Fig. 8a. In January and February, the fishing hotspot areas were mainly in the East China Sea, near the coastline from southern Jiangsu to northern Fujian Province. In March and April, the hotspot areas in the East China Sea and the South China Sea expanded. In May, the fishing hotspot areas in the East China Sea and the South China Sea decreased due to the fishing moratorium policy (Table 1). In June and July, fishing activities in the study area almost stopped, while a few illegal fishing activities continued. In August, fishing

Fig. 5 Total fishing and vessel hours per vessel and fishing ratio. **a** Interannual and **b** intra-annual variations in total vessel hours per vessel mt_v and total fishing hours per vessel mt_f in the study area during 2013–2018.

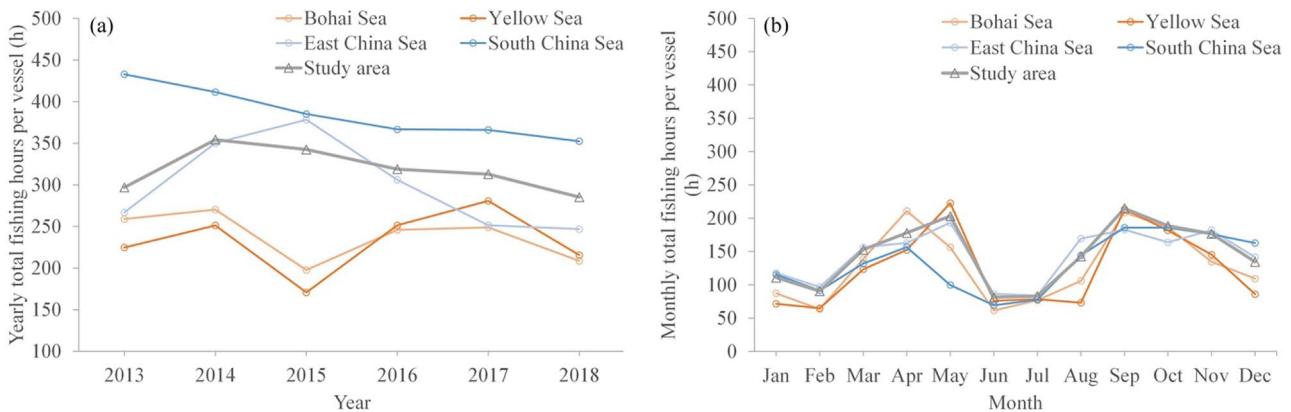
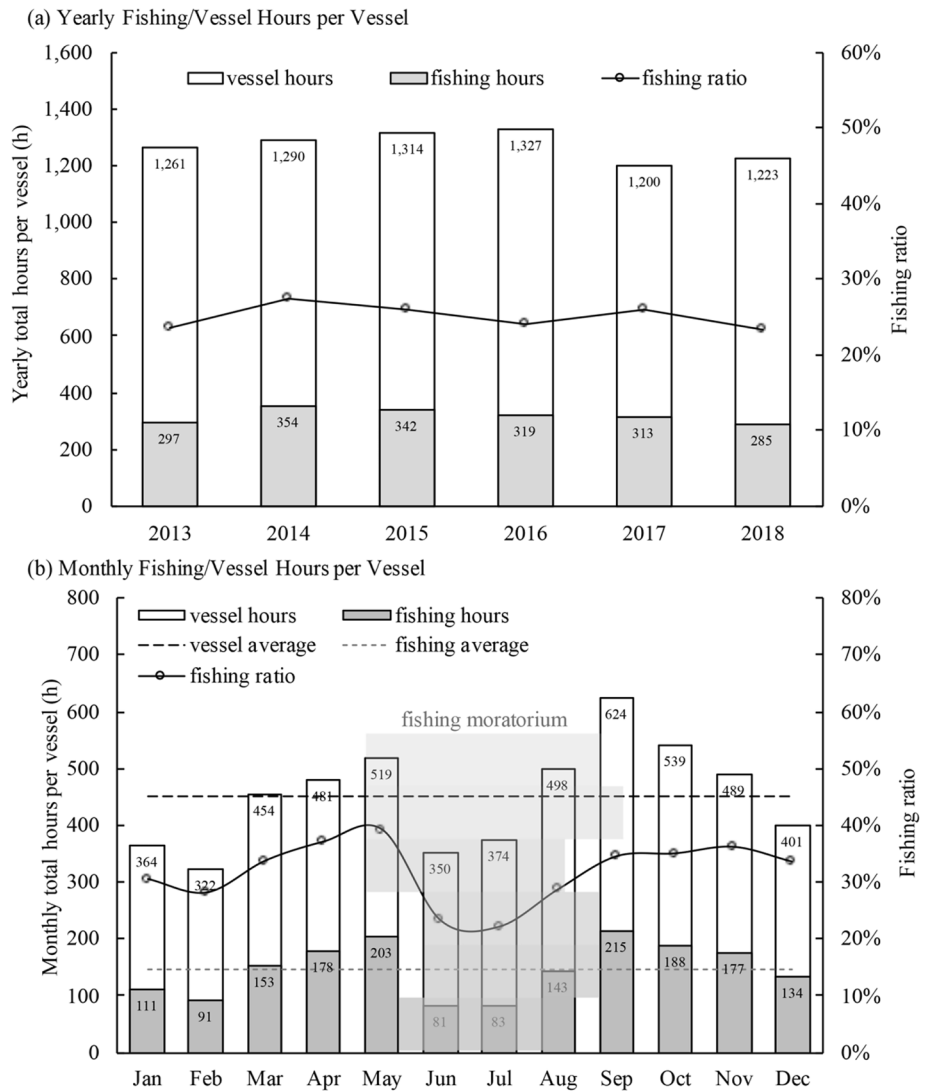


Fig. 6 Regional total fishing hours per vessel in the four seas of China. **a** Interannual trends of yearly total fishing hours per vessel and **b** intra-annual trends of total fishing hours per vessel in the four seas of China during 2013–2018.

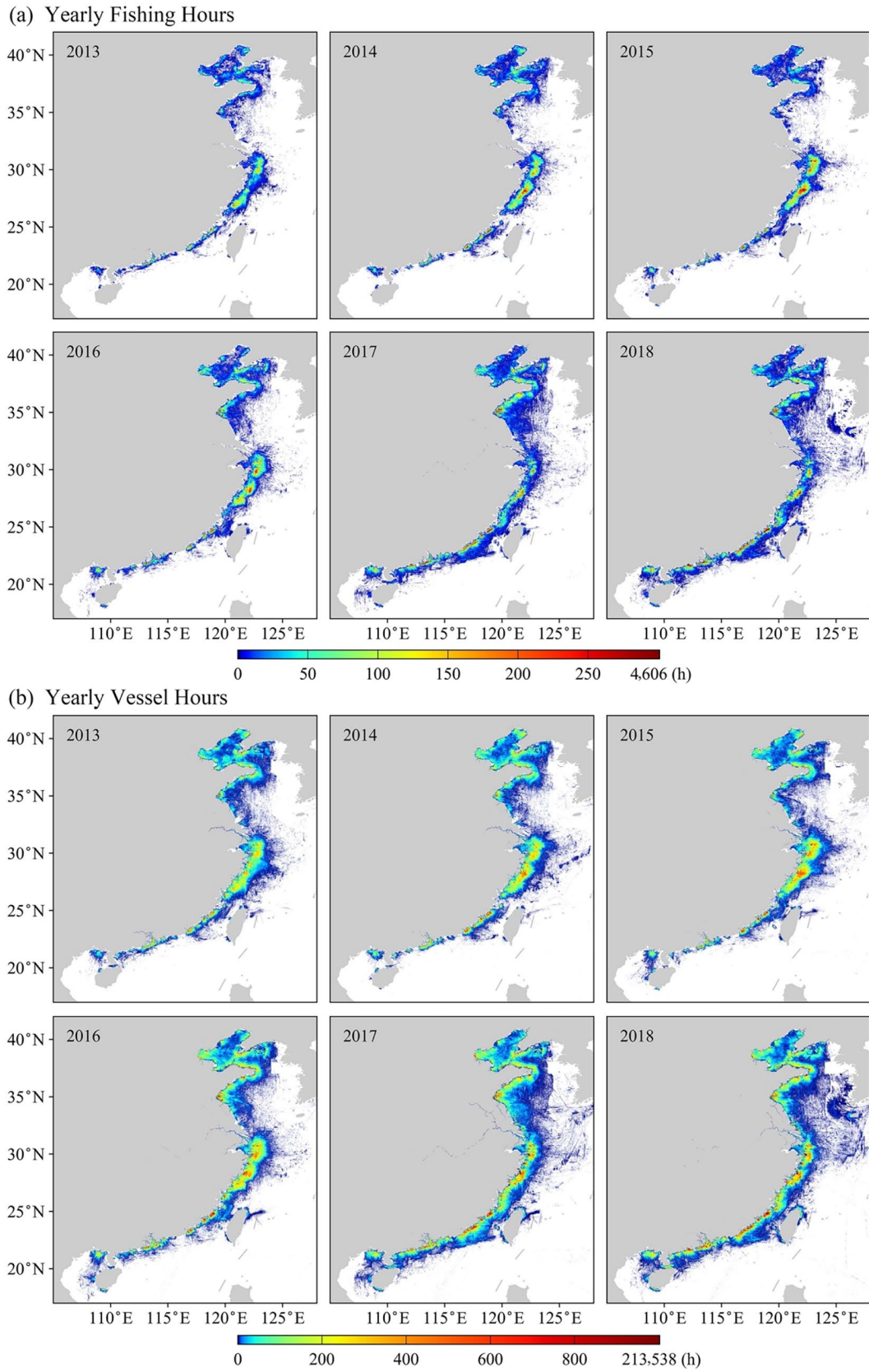


Fig. 7 Annual spatial patterns of China’s maritime fishing industry during 2013–2018: **a** yearly total fishing hours and **b** yearly total vessel hours

(a) Monthly Fishing Hours

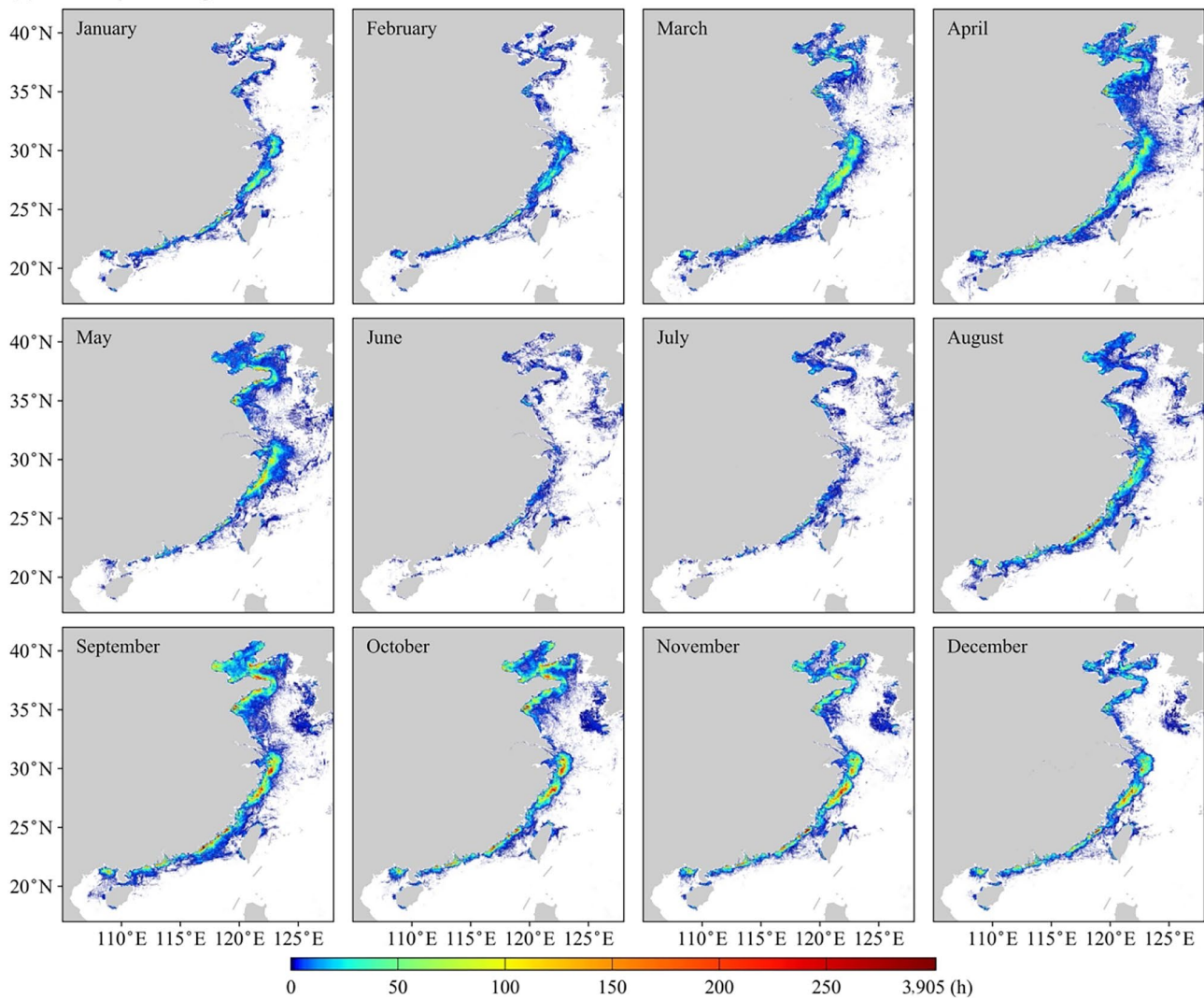


Fig. 8 Monthly spatial patterns of China's maritime fishing industry during 2013–2018: **a** monthly total fishing hours and **b** monthly total vessel hours

activities began to recover. In September, October, and November, the extent of fishing hotspot areas in the four seas reached the highest level of the year. In December, the fishing hotspot areas in the Bohai Sea and the Yellow Sea decreased slightly.

The spatial patterns of the monthly total vessel hours are shown in Fig. 8b, and the results are similar to the fishing hours.

4.2 Impact of Tropical Cyclones (TCs) on Fishing Vessel Activities

The total absolute impacts of the 52 TCs in China on the fishing hours (Δt_f) and vessel hours (Δt_v) from 2013 to 2018 are shown in Fig. 9. Due to the impacts of the TCs,

the absolute reductions in the fishing hours and vessel hours are mainly distributed in the East China Sea and the South China Sea (blue in Fig. 9).

The integrated reduction in fishing hours and vessel hours in the 52 TCs impact period during the 6 years was calculated as well and their percentage relative to the total fishing and vessel hours of the study area during the 6 years are 2.28% and 1.04%, respectively.

The total IR_f , total IR_v , mean IR_f , and mean IR_v statistics are shown in Fig. 10. The highest values of the annual total IR_f and IR_v were in 2013, and the highest values of the annual mean IR_f and IR_v were in 2015. The monthly total IR_f and IR_v reached the maximum in July, followed by August and September.

(b) Monthly Vessel Hours

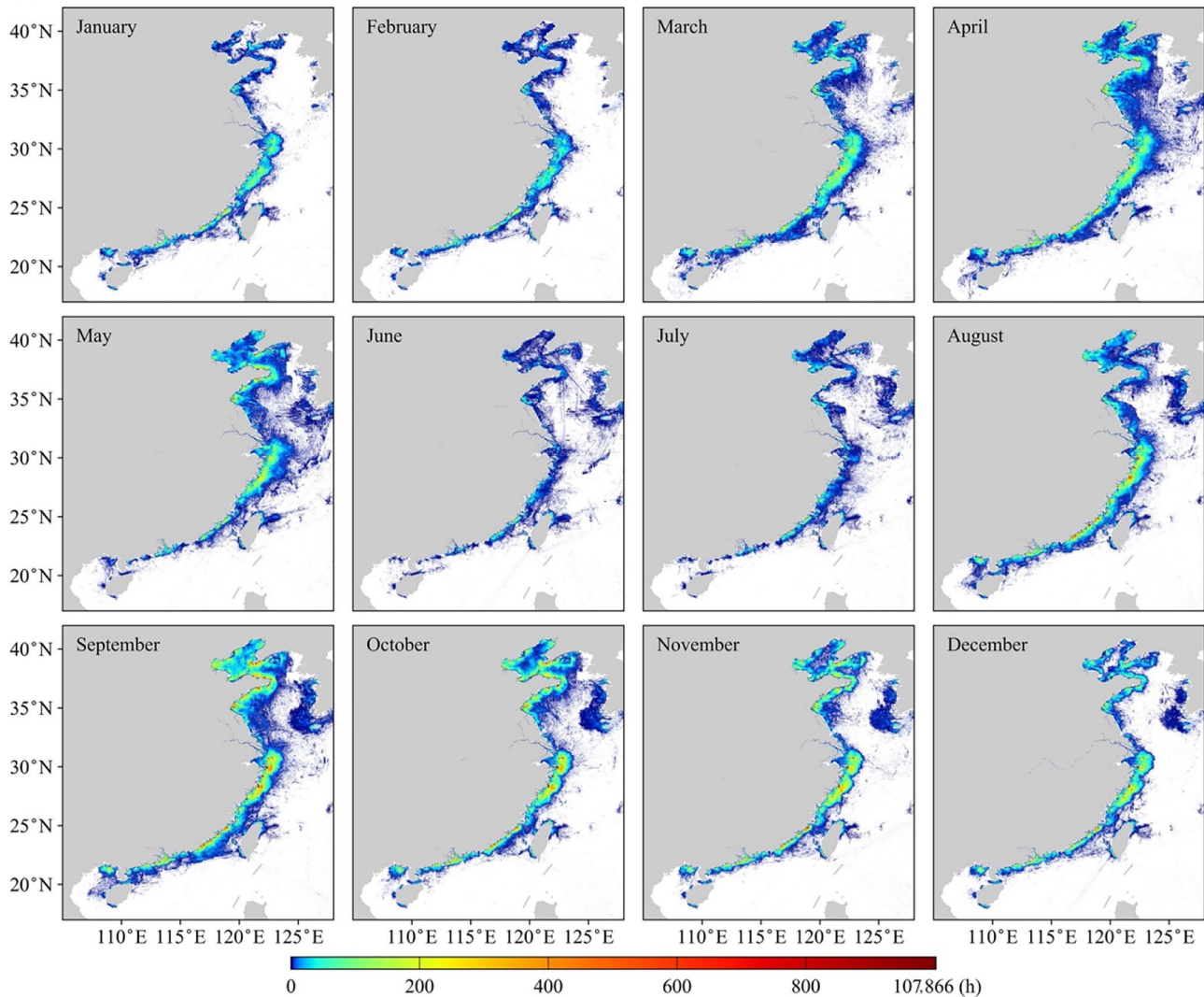


Fig. 8 (continued)

The TC landfall points and their corresponding IR_f and IR_v from 2013 to 2018 are shown in Fig. 11. It can be seen that (1) the landfall points of the TCs were over the coastline between 13°N and 32°N during the 6 years; and (2) the total IR_f and IR_v in each 1° interval showed a trend of increasing first and then decreasing as the latitude decreased from 32°N to 13°N , and the highest values of the total IR_f and IR_v appeared in the range of 22°N – 23°N .

Table 2 provides information on the 10 TCs with the highest IR_f values. The table suggests the following characteristics of TCs that caused the most disruption to fishing: (1) Six TCs landed when the fishing moratorium near the landfall site had expired; (2) The minimum and maximum latitudes of the 10 TC landfall points are 18.8°N (near Wenchang, Hainan Province) and 26°N (near Fuzhou, Fujian Province); (3) The maximum CWI and the minimum CWI

for the 10 TCs were 48.0 and 11.8, respectively, which demonstrates a medium range of variation; (4) The 10 TCs had a relative impact on the fishing hours (IR_f) of over 94% and a relative impact on the vessel hours (IR_v) of over 59%.

4.3 Hazard Index of Tropical Cyclones (TCs)

The interannual changes in the numbers and total CWI of the TCs are shown on the left of Fig. 12. 2013 and 2018 had the largest number of TCs, and the total CWI reached its maximum in 2013. The lowest number of TCs was in 2015, while in this year, the mean event CWI was the highest of all the years. In 2017, the yearly total CWI and the mean event CWI were both the minimum out of the 6 years despite the large number of TCs.

Fig. 9 Distribution of the total absolute impact indices of tropical cyclones in Northwest Pacific Waters on **a** fishing hours Δt_f and **b** vessel hours Δt_v during 2013–2018

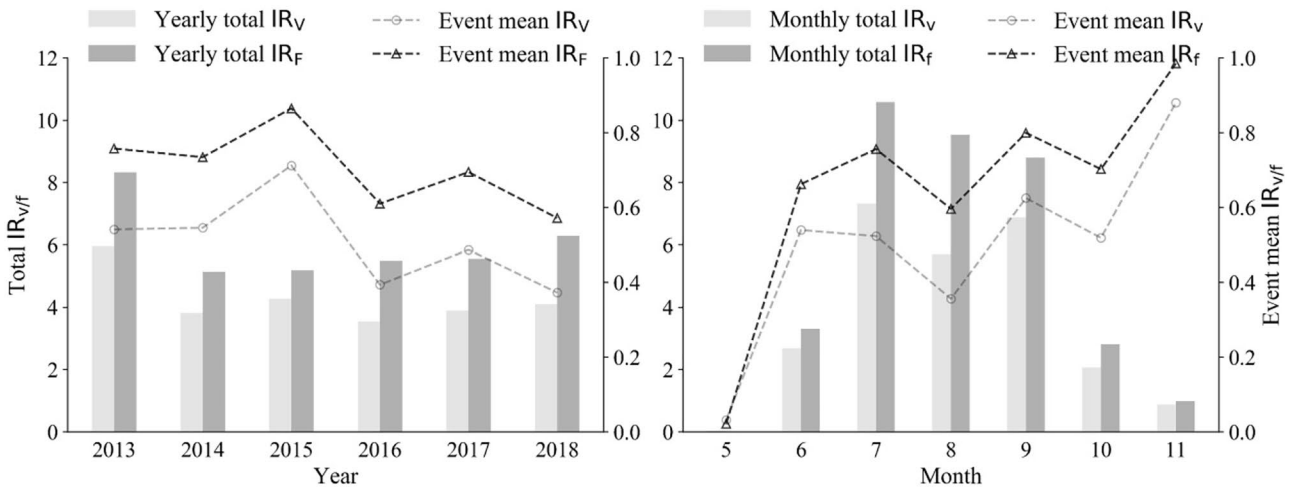
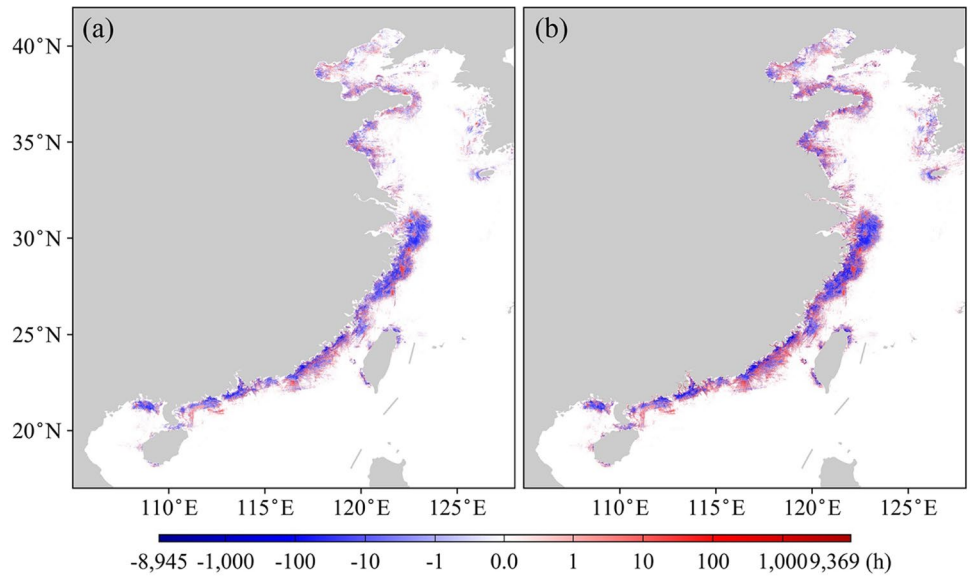


Fig. 10 Relative impact indices of the 52 tropical cyclones (TCs) studied on the fishing hours IR_f and vessel hours IR_v summed by year and month

Fig. 11 Tropical cyclone wind hazard index (CWI) and relative impact on fishing hours (IR_f) and vessel hours (IR_v) aggregated by the latitudes of the landfall points. Event IR_f is the IR_f of every single historical TC event. Mean IR_f is the average IR_f of TC events that the longitude of landfall points lies in every 1° range. Total IR_f is the sum of IR_f of TC events that the longitude of landfall points lies in every 1° range. So are IR_v and CWI .

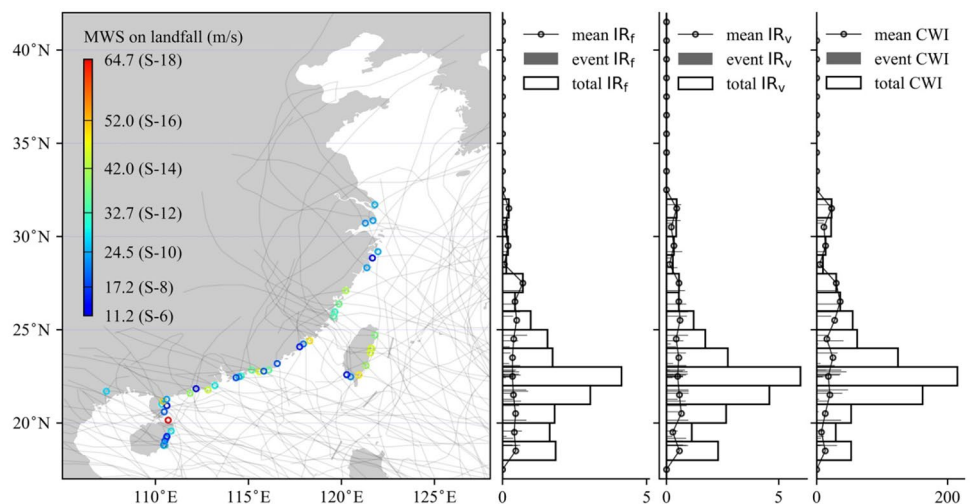


Table 2 Tropical cyclones (TCs) of the top 10 relative impact on fishing hours (IR_f)

ID	Name	D_L	Lat_L	D_{exp}	ΔT_f (h)	ΔT_v (h)	CWI	IR_f	IR_v
201311	Utor	2013/08/14	21.6	8/01	2711	6422	39.4	0.99	0.89
201334	Haiyan	2013/11/11	21.7	8/01	1456	2944	19.1	0.99	0.88
201826	Mangkhut	2018/09/16	21.8	8/16	20870	47736	48.0	0.98	0.79
201410	Rammasun	2014/07/18	20.1	8/01	405	986	37.4	0.97	0.68
201623	Sarika	2016/10/18	18.8	8/01	5365	10679	31.3	0.97	0.75
201307	Soulik	2013/07/13	26.0	8/01	3472	8050	32.6	0.96	0.59
201306	Rumbia	2013/07/01	21.0	8/01	293	942	11.8	0.96	0.72
201710	Nesat	2017/07/29	24.7	8/16	12006	36683	18.0	0.96	0.75
201418	Kalmaegi	2014/09/17	22.6	8/01	5187	9523	36.9	0.95	0.84
201320	Usagi	2013/09/22	22.7	8/01	6543	13798	45.6	0.94	0.82

D_L : Landfall date, Lat_L : Landfall latitude, D_{exp} : Local fishing moratorium expiration date

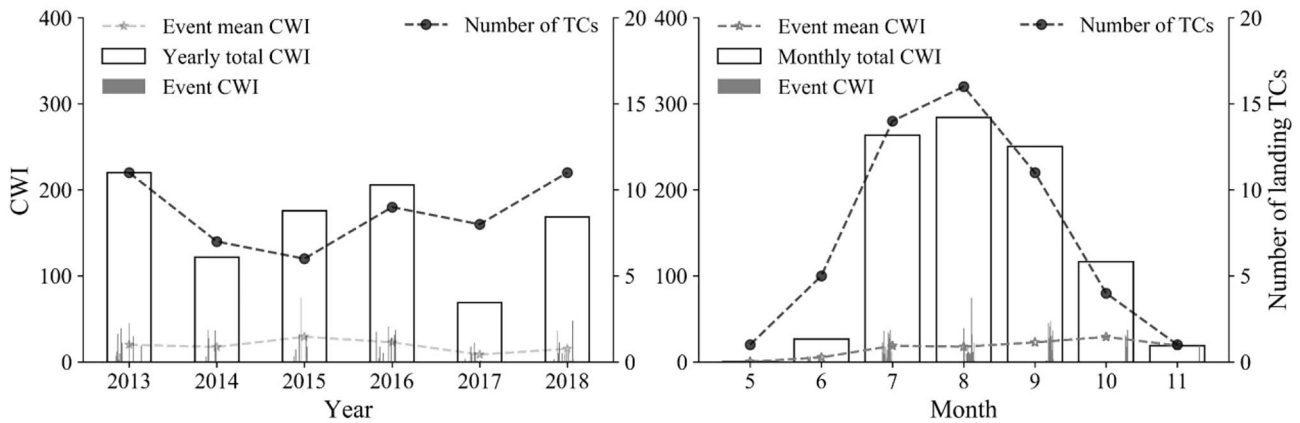


Fig. 12 Tropical cyclone (TC) numbers and cyclone wind hazard index (CWI) summed by year and month from 2013 to 2018

The intra-annual changes in the numbers and total CWI of the TCs are shown on the right of Fig. 12. The top three months with the largest numbers and the highest total CWI are July, August, and September, while no more than one TC event per month appeared from November to May during the 6 years. However, due to the super TC Haiyan in 2013, the monthly total CWI in November was not the lowest.

The spatial distribution of the CWI of the TCs from 2013 to 2018 is shown in Fig. 11. It can be seen that the landfall points are distributed on the coastline between 13°N–32°N. From 32°N to 13°N, the total CWI in each 1° interval increased first and then decreased. In 22°N–23°N, the landfall points (near Guangdong Province) within the interval correspond to the highest total CWI, and the landfall point with the highest event CWI also lies in 22°N–23°N.

4.4 Relationship Between Impact Indices and Hazard Index

The Pearson correlation coefficient and Spearman rank correlation coefficient were used to find the correlation between

Table 3 Correlation coefficients between IR_f , IR_v , and CWI using the correlation coefficient tests of Pearson and Spearman

	Pearson correlation coefficient		Spearman rank correlation coefficient	
	IR_f	IR_v	IR_f	IR_v
Correlation	0.5022	0.4542	0.5994	0.4769
P value	0.0002	0.0009	0.0000	0.0005

IR_f , IR_v , and CWI. The results are shown in Table 3. The Pearson correlation test and the Spearman rank correlation test have both passed the 0.01 significance level ($P < 0.01$). This suggests that both IR_f and IR_v are significantly related to CWI.

Log-normal CDF is used to fit the relationship between IR_f , IR_v , and CWI. The fitting results are shown with a solid red line in Fig. 13. The goodness-of-fit is measured by R^2 . It can be seen that (1) when $CWI < 5$, both curves are in a rapid growth stage, showing a near-vertical growth trend; (2) when $5 \leq CWI < 10$, the curves are in a transition stage,

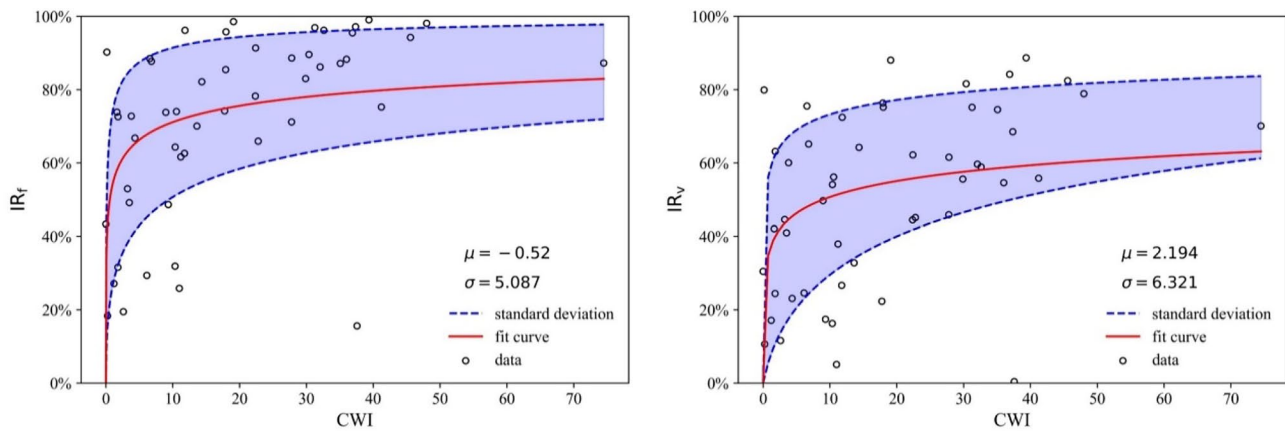


Fig. 13 Scatters (black circles) and fitted log-normal CDF curves (red line) of CWI vs IR_f (left, $R^2 = 0.207$) and IR_v (right, $R^2 = 0.135$) of 52 historical TCs. The blue dashed lines are the fitted log-normal CDF curves of the mean $IR_{fv} \pm$ standard deviation.

and the growth rates of IR_f and IR_v gradually slow down with the growth of CWI ; (3) when $CWI \geq 10$, the two curves are in a slow growth stage, and the growth rates of IR_f and IR_v tend to be stable and close to 0; and (4) under the same CWI , $IR_f > IR_v$.

The upper and lower standard deviation ranges of IR_f and IR_v are calculated by sections and fitted with a log-normal CDF curve. The results are shown by the blue dotted line in Fig. 13. It shows that (1) when $CWI < 5$, the dispersion degrees of IR_f and IR_v are the largest; (2) when $CWI \geq 5$, the dispersion degrees of IR_f and IR_v gradually decrease as CWI increases, which is mainly reflected by the lower bound of the double standard deviation range gradually approaching the mean value; and (3) under the same CWI , the dispersion degree of IR_f is less than that of IR_v .

5 Discussion

This study provides a quantitative relationship between the specified TC hazard index and the indices of impact on fishing vessel activities. Based on this relationship, the pre-cyclone impact assessment can be conducted to support fishing vessel management. Besides, compared to previous studies on TC impacts on fishing activities or losses in China (Ren 2009; Han et al. 2016), which were based on national and provincial units in annual or multiannual periods, this study provides the assessment with higher spatial resolution based on each individual TC event.

Although the spatiotemporal patterns of fishing activities and the impact of TC avoidance have been explored based on objective data derived from observed Automatic Identification System (AIS) data, it should be noted that the fishing activity data used in this study may have underestimated fishing intensity and vessel numbers, especially for small

vessels. The reason is that according to the International Maritime Organization only international sailing ships with a weight of more than 300 gross tons and non-international ships with a weight of more than 500 gross tons are obligated to install AIS (IMO 2004). Based on official Chinese statistics, the number of small fishing and motorized fishing vessels with a length of less than 12 m accounts for more than 50% of the total fishing fleet in China (MARA 2017). At the same time, only approximately 0.4% of small fishing vessels are equipped with AIS (Kroodsma et al. 2018). Therefore, underestimation of fishing activities must be considered or calibrated before further application, and the fusion of statistical data and AIS data should be explored in future studies.

6 Conclusion

Very few studies on the impacts of tropical cyclone (TC) avoidance to the vessel and fishing hours can be found, because quantitative fishing hour data at the regional and global scales were barely available or very challenging to extract in the past (Kroodsma et al. 2018). In this study, the analysis of the spatiotemporal patterns of fishing activities by vessel and fishing hours during 2013–2018 derived from AIS data was first implemented. Then the cyclone wind hazard index (CWI) was proposed to reflect the comprehensive TC hazard intensity. Two impact indices, IR_f and IR_v , were defined to reflect the influence of TC avoidance on fishing activities. Based on the data of 52 historical TCs, the relationship between the impacts on vessel activities and the fishing activities due to TC avoidance and TC wind hazard index were quantified. The main findings of this study have been summarized as below:

1. Most fishing activities took place from September to November after the fishing moratorium, and the overall fishing activity levels near China's offshore area have experienced an overall increase first and then a subsequent decrease because of the enhanced fishing regulations in China introduced in 2015. The most active fishing area throughout the year was located in the South China Sea, where the number of fishing hours per vessel has dropped by approximately 18.6%. However, in some other areas, such as the South China Sea and the Yellow Sea, the spatial extent of fishing hotspot areas has expanded.
2. The proposed TC hazard index *CWI* considers the integrated effects of wind speed on the temporal and spatial dimensions based on the 1 km wind field dataset of every six hours simulated with parametric wind field models. Based on the impact indices IR_f and IR_r , the highest hazard index and impact indices, excluding the fishing moratorium period, occurred in September. The area with the largest hazard index and relative impact index values is located offshore near Guangdong Province, which was hit by frequent TCs in the study period.
3. Both impact indices have statistically significant correlations with *CWI* as an independent variable and were fitted with the cumulative probability function (CDF) of the log-normal distribution.

The relationship between *CWI* and the impact on fishing vessel activity can be used in a variety of disaster management applications. For example, the quantitative findings of this study can help improve emergency response decision making. An optimal avoidance routes can be solved and disseminated to fishing vessels through satellite-based tele-communication system by the authority, according to the assessment on the costs of different vessel avoidance route scenarios. Another possible application is that it can be used in fishing insurance product design. The major risk metrics of fishing activity interruption, including the loss probability distribution, the expected annual loss, and the variation of loss, can be estimated based on the quantitative relationship between *CWI* and fishing activities, the spatiotemporal pattern of fishing activities, and other datasets such as historical TC tracks, and so on.

Acknowledgements This work was mainly supported by the National Key Research and Development Program of China (Grant Nos. 2018YFC1508803 and 2017YFA0604903) and jointly supported by the Key Special Project for Introduced Talents Team of the Southern Marine Science and Engineering Guangdong Laboratory (Guangzhou) (Grant No. GML2019ZD0601).

Open Access This article is licensed under a Creative Commons Attribution 4.0 International License, which permits use, sharing, adaptation, distribution and reproduction in any medium or format, as long as you give appropriate credit to the original author(s) and the source,

provide a link to the Creative Commons licence, and indicate if changes were made. The images or other third party material in this article are included in the article's Creative Commons licence, unless indicated otherwise in a credit line to the material. If material is not included in the article's Creative Commons licence and your intended use is not permitted by statutory regulation or exceeds the permitted use, you will need to obtain permission directly from the copyright holder. To view a copy of this licence, visit <http://creativecommons.org/licenses/by/4.0/>.

References

- Anticamara, J.A., R. Watson, A. Gelchu, and D. Pauly. 2011. Global fishing effort (1950–2010): Trends, gaps, and implications. *Fisheries Research* 107(1–3): 131–136.
- China Weather. 2010. Tropical cyclone numbering, locating and warning map. China. <http://www.weather.com.cn/typhoon/tfzs/04/397397.shtml>. Accessed 1 Jul 2022 (in Chinese).
- CMA (China Meteorological Administration). 2007. Measures for issuing and disseminating meteorological disaster early warning signals. Beijing, China: CMA. http://www.cma.gov.cn/2011/zwxw/2011/zxflfg/2011/zgfwj/201208/t20120803_180761.html. Accessed 20 Jul 2020 (in Chinese).
- CME (Chicago Mercantile Exchange) Group. 2009. CME Hurricane index futures and options. USA. https://www.cmegroup.com/trading/weather/files/WT106_NEWHurricaneFC.pdf. Accessed 1 Jul 2022.
- Elsberry, R.L. 1987. *A global view of tropical cyclones*. Monterey, CA: Office of Naval Research.
- Emanuel, K. 2005. Increasing destructiveness of tropical cyclones over the past 30 years. *Nature* 436(7051): 686–688.
- Fang, W., and X. Shi. 2012. A review of stochastic modeling of tropical cyclone track and intensity for disaster risk assessment. *Advances in Earth Science* 27(8): 866–875 (in Chinese).
- Gelchu, A., and D. Pauly. 2007. *Growth and distribution of port-based fishing effort within countries' EEZ from 1970 to 1995*. Fisheries Centre Research Reports 15(4). <https://s3-us-west-2.amazonaws.com/legacy.seaaroundus/doc/Researcher+Publications/dpauly/PDF/2007/Books%26Chapters/GrowthDistributionPartBasedFishingEffort.pdf>. Accessed 12 Dec 2020.
- Georgiou, P.N., A.G. Davenport, and P.J. Vickery. 1983. Design wind speeds in regions dominated by tropical cyclones. *Journal of Wind Engineering and Industrial Aerodynamics* 13(1–3): 139–152.
- Guet, J., E. Galbraith, D. Kroodsma, and B. Worm. 2019. Seasonal variability in global industrial fishing effort. *PLoS ONE* 14(5): Article e0216819.
- Han, X., Y. Li, and Z. Yue. 2016. On risk evaluation and zoning of typhoon disaster to fishery in China. *Ocean Development and Management* 33(5): 64–69 (in Chinese).
- IMO (International Maritime Organization). 2004. *International convention for the safety of life at sea (SOLAS)*. <https://news.magnify.it/wp-content/uploads/2017/08/SOLAS-International-Convention-for-the-safety-of-life-at-sea-2004.pdf>. Accessed 20 Oct 2020.
- Jovel, J.R., and M.S. Mudahar. 2010. *Damage, loss, and needs assessment guidance notes (Vol. 2): Conducting damage and loss assessments after disasters (Chinese)*. Washington, DC: World Bank Group. <http://documents.worldbank.org/curated/en/837041468336025149/Conducting-damage-and-loss-assessments-after-disasters>. Accessed 20 Oct 2020.
- Knapp, K.R., M.C. Kruk, D.H. Levinson, H.J. Diamond, and C.J. Neumann. 2010. The international best track archive for climate stewardship (IBTrACS) unifying tropical cyclone data. *Bulletin of the American Meteorological Society* 91(3): 363–376.

- Kroodtsma, D.A., J. Mayorga, T. Hochberg, N.A. Miller, K. Boerder, F. Ferretti, B. Worm, and B. Bergman et al. 2018. Tracking the global footprint of fisheries. *Science* 359(6378): 904–907.
- Li, Y., and W. Fang. 2012. A rapid loss index for tropical cyclone disasters in China. In *Proceedings of the 2012 Fifth International Joint Conference on Computational Sciences and Optimization*, 23–26 June 2012, Harbin, China, 747–750.
- Lin, W., and W. Fang. 2013. Regional characteristics of Holland B parameter in typhoon wind field model for Northwest Pacific. *Tropical Geography* 33(2): 124–132 (in Chinese).
- MARA (Ministry of Agriculture and Rural Affairs of the People's Republic of China). 2017. *China fishery statistical yearbook 2016*. Beijing, China: MARA (in Chinese).
- MARA (Ministry of Agriculture and Rural Affairs of the People's Republic of China). 2018a. *China fishery statistical yearbook 2017*. Beijing, China: MARA (in Chinese).
- MARA (Ministry of Agriculture and Rural Affairs of the People's Republic of China). 2018b. *Notice on the adjustment of the marine fishing moratorium system*. Beijing, China: MARA. http://www.moa.gov.cn/gk/zcfg/nybgz/201802/t20180209_6136812.htm. Accessed 1 May 2022 (in Chinese).
- Meng, Y., M. Matsui, and K. Hibi. 1997. A numerical study of the wind field in a typhoon boundary layer. *Journal of Wind Engineering and Industrial Aerodynamics* 67–68: 437–448.
- MNR (Ministry of Natural Resources of the People's Republic of China). 2019. *National marine economic statistics bulletin 2018*. Beijing, China: MNR. http://gi.mnr.gov.cn/201904/t20190411_2404774.html. Accessed 20 July 2020 (in Chinese).
- Mo, W., and W. Fang. 2016. Empirical vulnerability functions of building contents to flood based on post-typhoon (Fitow, 201323) questionnaire survey in Yuyao, Zhejiang. *Tropical Geography* 36(4): 633–641 (in Chinese).
- MOF (Ministry of Finance of the People's Republic of China). 2015. *Notice on the adjustment of domestic fishing and aquaculture oil price subsidy policies to promote the sustained and healthy development of fisheries*. Beijing, China: MOF. http://www.mof.gov.cn/gp/xxgkml/jjss/201507/t20150709_2512172.html. Accessed 10 Oct 2020.
- Monteclaro, H., G. Qunitio, M.A. Dino, R. Napata, L. Espectato, K. Anraku, K. Watanabe, and S. Ishikawa. 2018. Impacts of Typhoon Haiyan on Philippine capture fisheries and implications to fisheries management. *Ocean & Coastal Management* 158: 128–133.
- Owens, B., and G. Holland. 2010. The Willis Hurricane Index. In *Proceedings of 29th Conference on Hurricanes and Tropical Meteorology*, 10–14 May 2010, Tucson, AZ, USA. <https://ams.confex.com/ams/29Hurricanes/webprogram/29HURRICANES.html>. Accessed 1 Jul 2022.
- Porter, K. 2021. A beginner's guide to fragility, vulnerability, and risk. In *Encyclopedia of earthquake engineering*, ed. M. Beer, I.A. Kougoumtzoglou, E. Patelli, and S.K. Au, 4–10. Heidelberg: Springer.
- Ren, F., Y. Wang, X. Wang, and W. Li. 2007. Estimating tropical cyclone precipitation from station observations. *Advances in Atmospheric Sciences* 24(4): 700–711.
- Ren, L. 2009. *Assessment for the loss of income of fishermen caused by storm surge disaster*. Master's thesis. Qingdao, China: Ocean University of China (in Chinese).
- Tan, C., and W. Fang. 2018. Mapping the wind hazard of global tropical cyclones with parametric wind field models by considering the effects of local factors. *International Journal of Disaster Risk Science* 9(1): 86–99.
- Vickery, P.J., and D. Wadhera. 2008. Statistical models of Holland pressure profile parameter and radius to maximum winds of hurricanes from flight-level pressure and H*Wind data. *Journal of Applied Meteorology and Climatology* 47(10): 2497–2517.
- Watson, R.A., W.L. Cheung, J.A. Anticamara, R.U. Sumaila, D. Zeller, and D. Pauly. 2013. Global marine yield halved as fishing intensity redoubles. *Fish and Fisheries* 14(4): 493–503.
- Xu, M., Q. Yang, and M. Ying. 2005. Impacts of tropical cyclones on Chinese lowland agriculture and coastal fisheries. In *Natural disasters and extreme events in agriculture: Impacts and mitigation*, ed. M.V.K. Sivakumar, R.P. Motha, and H.P. Das, 137–144. Heidelberg: Springer.
- Ying, M., W. Zhang, H. Yu, X. Lu, J. Feng, Y. Fan, Y. Zhu, and D. Chen. 2014. An overview of the China Meteorological Administration tropical cyclone database. *Journal of Atmospheric and Oceanic Technology* 31(2): 287–301.
- Yu, J., D. Tang, G. Chen, Y. Li, Z. Huang, and S. Wang. 2014. The positive effects of typhoons on the fish CPUE in the South China Sea. *Continental Shelf Research* 84: 1–12.
- Zheng, Q., W. Fan, X. Wang, W. Li, Q. Zhang, and S. Zhang. 2016. Typhoon status of offshore fishing grounds in China and its impact analysis on fishing boats. *Marine Science Bulletin* 35(2): 225–234 (in Chinese).